NMR Loschmidt echoes as quantifiers of decoherence in interacting spin systems

C. M. Sánchez, P. R. Levstein, R. H. Acosta, and A. K. Chattah*

Facultad de Matemática, Astronomía y Física, UNC and IFFAMAF (CONICET), Ciudad Universitaria, X5016LAE Córdoba, Argentina

(Received 8 May 2009; published 27 July 2009)

In this work we present solid-state nuclear magnetic-resonance experiments to study decoherence in the dynamics of many-spin systems. We characterize the global Loschmidt echo and the distribution of multiple-quantum coherence orders during the evolution under dipolar and double-quantum Hamiltonians. To study an infinite ^{1}H system and a closed cluster of nuclear spins we use polycrystalline adamantane and the liquid crystal 5CB in the nematic mesophase, respectively, as model systems. The infinite or finite nature of the system is clearly manifested through spin counting measurements. Comparison between experimental and numerical results gives insights on the decoherence mechanisms in these systems. Contrastingly, the dominating mechanism in 5CB affects all coherence orders in the same way, while in adamantane higher orders of coherence decay faster than the lower ones.

DOI: 10.1103/PhysRevA.80.012328 PACS number(s): 03.67.Pp, 03.65.Yz, 76.60.Lz, 76.90.+d

I. INTRODUCTION

The study of generation, evolution, and control of coherent quantum dynamics in large Hilbert spaces has drawn much theoretical and experimental attention over the last years due to the direct application on, for instance, quantum information processing [1–3] and spintronics [4]. The main drawback on the implementation of quantum registers arises from the degradation of the correlation between states due to interactions with the environment. This process is generally known as decoherence and it determines how much information can be transmitted from one quantum manipulation to the next [5–9]. In particular, solid state nuclear magnetic resonance (NMR) is a very suitable technique to study decoherence during the dynamics of open quantum systems constituted by dipolar coupled nuclear spins. Then, the loss of information due to interaction with uncontrolled degrees of freedom can be characterized [10–14]. In particular, multiple-quantum NMR experiments can be used to create correlated multispin states. By monitoring the creation and evolution of the different multiple-quantum coherences (MQC) a great deal of information ranging from cluster sizes, Hilbert space connectivity, and decoherence processes can be obtained [15–22]. Nevertheless, the NMR signal attenuation arises not only from the system decoherence, but also from pulse sequence imperfections that are inherent to every experiment. The most general approach is to optimize the pulse sequence design in order to minimize its influence on the observation of the quantum evolution of the system. This often leads to long unitary blocks of radio frequency (rf) pulses to generate the desired average Hamiltonian, as in the case of the Baum-Pines sequence and further corrected schemes [17,23,24]. This may be a drawback on the study of strongly dipolar coupled systems, where the evolution at very short times contains relevant information, as in the cases to be treated here.

In this work, we focus on experimental implementation of Loschmidt echoes (LE) as quantifiers of decoherence in many-body spin systems. The LE are generated by reversing a given time evolution of the system through a change in the sign of the Hamiltonian [25]. Implementations with different Hamiltonians and systems can yield information to distinguish intrinsic decoherence induced by the own interactions of the system, from that arising on experimental imperfections [13,14].

We probe the spin dynamics with two different Hamiltonians: a rotated dipolar Hamiltonian, $\mathcal{H}_{xx} \propto (2I_j^x I_k^x - I_j^z I_k^z - I_j^y I_k^y)$, and a double-quantum Hamiltonian $\mathcal{H}_{DQ} \propto (I_j^+ I_k^+ + I_j^- I_k^-)$, on two well differentiated spin systems. One of the systems is polycrystalline adamantane, which involves an infinite spin 1/2 network where there are only intermolecular dipolar interactions. The other one is the liquid crystal 4-n-pentyl-4′-cyanobiphenyl (5CB), in the nematic phase where only intramolecular dipolar interactions survive giving rise to a closed system of a finite number of spins. The spin system dynamics are analyzed by comparing the evolution of MQC for each situation [15].

II. DIPOLAR AND DOUBLE-QUANTUM EVOLUTIONS

The multiple-quantum coherence characterization of spin dynamics was analyzed by performing an evolution of the system under the secular dipolar, $\mathcal{H}_{xx}$, and double quantum, $\mathcal{H}_{DQ}$, Hamiltonians. We follow the usual MQ encoding based on a preparation and mixing (or reversion) periods, combined with phase-shift incrementation of the radiofrequency pulses [15–17].

In a strong magnetic field $\mathbf{B}_0$ in the z direction, an N spin-1/2 system has 2^N stationary states. These can be classified according to the magnetic quantum number $M_z = \Sigma_i m_{zi}$ where $m_{zi} = \pm 1/2$ is the eigenvalue of the ith spin in the system. For nondegenerate stationary states there are 2^{2N-1} possible transitions of finite energy between any two levels. The difference in M_z values between the coupled states is referred to as the coherence number. On the other hand, when the state is expressed in the eigenbasis of the Zeeman system, the presence of a nonzero density-matrix element $\langle r|\rho|s\rangle$ indicates the presence of a n quantum coherence, where $n = M_z(r) - M_z(s)$. Then, a rotation around the

*chattah@famaf.unc.edu.ar

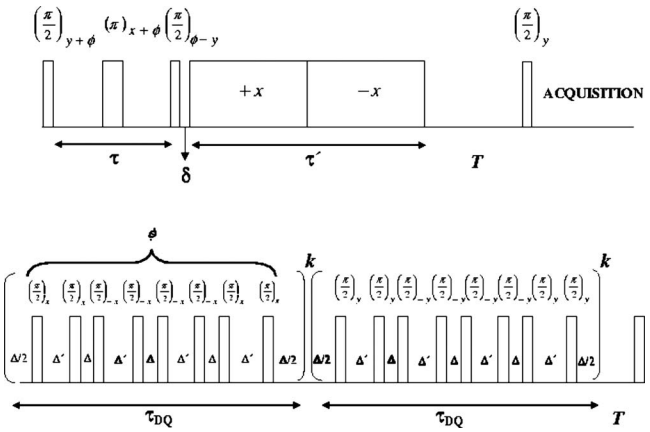

FIG. 1. Schematic representation of the pulse sequences used in this work. (a) τ is the evolution time under dipolar Hamiltonian $\mathcal{H}_{xx}$ and (b) τ_{DQ} is the evolution time under double-quantum Hamiltonian $\mathcal{H}_{DQ}$.

axis of quantization, $\hat{z}$, with an angle ϕ characterizes the order of coherence because $\langle r|\exp(-i\phi I^z)\rho\exp(i\phi I^z)|s\rangle = \exp(i\phi n)\langle r|\rho|s\rangle$ [26]. Here, I^α with $\alpha=x,y,z$ represents the components of the total angular momentum.

The multiple-quantum encoding of the different coherence orders on the dipolar evolution was made through a modified multiple-quantum NMR magic echo sequence, as schematized in Fig. 1(a). A similar approach was recently implemented by Cho *et al.* [18] for the investigation of many-spin dynamics of the NMR free-induction decay. Our preparation period, τ, is an evolution under $\mathcal{H}_{xx}$ while the magic echo used for the mixing period is an evolution with $[-\frac{1}{2}]\mathcal{H}_{xx}$. For a system of spins initially in equilibrium with the external magnetic field, the density matrix is $\rho(0)\propto I^z$. The propagator for the preparation period is written as

$$U_\phi(\tau) = \exp(-i\phi I^z)\exp\left(i\frac{\pi}{2}I^y\right)\exp(i\phi I^z) \times\exp[-i\tau(\mathcal{H}_Z+\mathcal{H}_{zz})/2\hbar]\exp(-i\phi I^z) \times \exp(-i\pi I^x)\exp(i\phi I^z)\exp[-i\tau(\mathcal{H}_Z+\mathcal{H}_{zz})/2\hbar] \times\exp(-i\phi I^z)\exp\left(-i\frac{\pi}{2}I^y\right)\exp(i\phi I^z),$$

where $\mathcal{H}_Z$ is the Zeeman Hamiltonian of the spin system and $\mathcal{H}_{zz}=\Sigma_{j<k}\hbar d_{jk}(2I_j^zI_k^z-I_j^xI_k^x-I_j^yI_k^y)$ is the secular dipolar term. The dipolar coupling-constant d_{jk} between spins j and k is

$$d_{jk} = \frac{\mu_0\gamma^2\hbar}{4\pi r_{jk}^3}\frac{[1-3\cos^2(\theta_{jk})]}{2}.$$

Here, γ is the gyromagnetic ratio, r_{jk} is the spin-spin distance, and θ_{jk} is the angle between the internuclear vector $\mathbf{r}_{jk}$ and the external field $\mathbf{B}_0$.

The π pulse around the x direction has the effect of refocusing the Zeeman term $\mathcal{H}_Z$. Then, the propagator at the preparation time τ involves the dipolar evolution under $\mathcal{H}_{xx}=\exp(i\pi/2I^y)\mathcal{H}_{zz}\exp(-i\pi/2I^y)$, rotated by ϕ around the z direction, as can be seen from the following lines,

$$U_\phi(\tau) = \exp(-i\phi I^z)\exp\left(i\frac{\pi}{2}I^y\right)\exp(-i\tau\mathcal{H}_Z/2\hbar) \times\exp(-i\tau\mathcal{H}_{zz}/2\hbar)\exp(+i\tau\mathcal{H}_Z/2\hbar)\exp(-i\tau\mathcal{H}_{zz}/2\hbar) \times\exp(-i\pi I^x)\exp\left(-i\frac{\pi}{2}I^y\right)\exp(i\phi I^z),$$

$$U_\phi(\tau) = \exp(-i\phi I^z)\exp(+i\tau\mathcal{H}_{xx}/\hbar) \times\exp\left(i\frac{\pi}{2}I^y\right)\exp(-i\pi I^x)\exp\left(-i\frac{\pi}{2}I^y\right)\exp(i\phi I^z),$$

$$U_\phi(\tau) = \exp(-i\phi I^z)\exp(i\tau\mathcal{H}_{xx}/\hbar)\exp(i\phi I^z)\exp(-i\pi I^z).$$

Since the operator $U_\phi(\tau)$ is applied to $\rho(0)\propto I^z$, the factor on the right is irrelevant because it commutes with I^z. The refocusing of the dipolar dynamics takes place during $\tau'\sim 2\tau$, under the presence of a spin-lock radio frequency field applied along $+x$ and $-x$ axis. Then, the effective dipolar Hamiltonian is given by $[-\frac{1}{2}]\mathcal{H}_{xx}$ [27]. The final density matrix is

$$\rho_\phi(\tau+\tau') = U_\phi^\dagger(\tau+\tau')I_zU_\phi(\tau+\tau'),$$

with the propagator

$$U_\phi(\tau+\tau') = \exp(-i\tau'\mathcal{H}_{xx}/2\hbar)\exp(-i\phi I^z)\exp(i\tau\mathcal{H}_{xx}/\hbar).$$

Then, the initial condition evolves under the dipolar Hamiltonian $\mathcal{H}_{xx}$ and afterwards a ϕ rotation around z encodes the multiple-quantum coherences created during this evolution in the Zeeman basis. The spin-lock field refocuses the multiple-spin terms back to observable single-quantum coherence terms. To acquire a signal, a final lecture pulse is applied after a time T that allows for decoherence in the plane. The observed signal, $S_\phi(\tau)$, is a function of the preparation time τ and the phase angle ϕ,

$$S_\phi(\tau) = \mathrm{Tr}[I^zU_\phi^\dagger(\tau+\tau')I^zU_\phi(\tau+\tau')] = \sum_n \exp(i\phi n)S_n(\tau),$$

where $S_n(\tau)$ is the coherence order distribution in the Zeeman basis, which can be obtained by Fourier transformation with respect to ϕ.

In order to encode quantum coherence orders during the evolution with a double-quantum Hamiltonian (DQ), we have used the well-known eight-pulse sequence shown in Fig. 1(b) [10,16,17], where the effective Hamiltonian is

$$\mathcal{H}_{DQ} = -\frac{1}{2}\sum_{j<k}\hbar d_{jk}(I_j^+I_k^+ + I_j^-I_k^-). \quad (1)$$

The encoding and observation of the different coherence orders, $S_n(\tau_{DQ})$, follows the same procedure as described before. The dipolar evolution under $\mathcal{H}_{xx}$ has a period that is 3/2 times shorter than the corresponding to $\mathcal{H}_{DQ}$. Thus, in order to compare evolutions we refer all data to τ, with $\tau=\frac{2}{3}\tau_{DQ}$ [28,29].

III. MATERIALS AND EXPERIMENTAL SETUP

The experiments were performed using a Bruker Avance II spectrometer operating at a ^{1}H resonance frequency of

300.13 MHz under static conditions. Experiments in adamantane were performed at room temperature while 5CB was maintained in the nematic mesophase at 300 K.

Adamantane forms a plastic crystal in which the nearly spherical molecules tumble rapidly and isotropically in the solid phase. The motion averages all the intramolecular dipolar couplings to zero but does not eliminate intermolecular couplings. However the motion leaves only one distinct coupling between every pair of molecules, reducing the adamantane molecule to a point-dipole source containing 16 spins packed into a face-centered-cubic lattice. The compound behaves as an infinite spin-pair system with an effective dipolar coupling $d/2\pi \simeq 5.7$ kHz [30].

Liquid crystal 5CB is composed by a cyano group, two aromatic rings, and an aliphatic chain of five carbons. In the nematic mesophase the molecular director is mostly aligned with the external magnetic field. Rotations and diffusion of the molecules eliminates intermolecular dipolar interactions [31]. For the purpose of MQC encoding, this compound can be considered as a finite system composed by 19 protons [17]. The main dipolar interactions occur between protons in the same aromatic ring where $d/2\pi \simeq 3.9$ kHz and between protons in the first methylene group of the chain, with $d/2\pi \simeq 4.9$ kHz [32].

In all the experiments, an free induction decay (FID) was recorded for each value of ϕ and τ. Each spectrum was integrated to give $S_\phi(\tau)$ and finally Fourier transformed to give the coherence distribution $S_n(\tau)$, at each preparation time τ. Signal $S_\phi(\tau)$ was normalized to a reference FID obtained by the application of a single pulse, $\pi/2=2.2$ μs. The phase ϕ was incremented with $\Delta\phi=2\pi/32$ for 5CB and $\Delta\phi=2\pi/64$ in adamantane, encoding up to 16 and 32 orders, respectively. In the pulse sequence corresponding to dipolar Hamiltonian [Fig. 1(a)], the power during the rf spin lock was set to $\omega_{1H}/2\pi=33$ kHz, in order to maximize the signal. In this sequence the preparation time τ ranged between 10 to 600 μs. Each corresponding echo time was $\tau'=2\tau+\varepsilon$, where ε was optimized to obtain the maximum refocused signal. The short delay $\delta \approx 1$ μs, between preparation and reversion blocks, was inserted to minimize pulse transients. In the sequence corresponding to double-quantum dynamics [Fig. 1(b)], the time delay between pulses was varied from 3 to 50 μs to increase the preparation time, τ_{DQ}, from 36 to 600 μs, using only one cycle ($k=1$), yielding the Hamiltonian $\mathcal{H}_{DQ,1}$ [19]. In adamantane these results were compared with two other groups of measurements, where the effective double-quantum Hamiltonian, $\mathcal{H}_{DQ,k}$, was generated by repeating k times a block with a fixed duration, $\tau_{DQ}^{\text{cycle}}=60$ μs and $\tau_{DQ}^{\text{cycle}}=120$ μs, respectively. Decoherence loss time before the lecture pulse was $T=1$ ms for all cases. Both pulse sequences develop only even coherence orders.

IV. RESULTS

A. Loschmidt echoes

In a multispin system, high coherence orders develop at the expense of lower ones and, as the evolution time increases, the system becomes highly correlated [10,20]. As the single quantum coherence is the only directly observable, the spread of information to higher orders leads to a decay of the NMR signal [16–18]. Nevertheless, if at a given time the information contained in the different coherence orders is accumulated, the information at $\tau=0$ should in principle be recovered [33]. The Loschmidt echo in the pulse sequences used in this work can be defined as $S_{LE}(\tau)=S_{\phi=0}(\tau)$. In fact, $S_{LE}(\tau)=\Sigma_n S_n(\tau)$, then the decay of this signal, is an ideal quantifier of the overall decoherence in a particular pulse sequence. Note that in the absence of decoherence $S_{LE}(\tau)=1$ for all times τ.

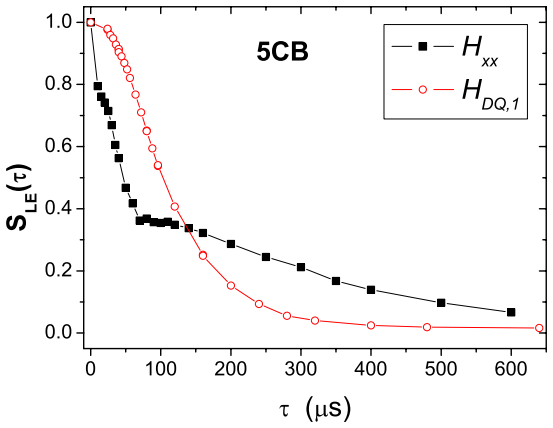

FIG. 2. (Color online) Loschmidt Echo, $S_{LE}(\tau)$, for dipolar and double-quantum pulse sequences in 5CB, normalized with a reference FID recorded after a $\pi/2$ pulse.

The decoherence affecting the evolution of a spin system is dependent on the chosen Hamiltonian, for instance a LE under a single-spin Hamiltonian, e.g., a Hahn echo, is different from the LE under a many-body Hamiltonian. In our experiments, we have an additional difference because we compare two many-body Hamiltonians, $\mathcal{H}_{xx}$ and $\mathcal{H}_{DQ}$, reversed by different techniques. The sequence to refocus $\mathcal{H}_{xx}$ includes a spin-lock yielding $-\mathcal{H}_{xx}/2+\Sigma$, where Σ represents nonsecular terms of the order d^2/ω_{1H}. In contrast, the sequence to measure the LE under $\mathcal{H}_{DQ}$ is exactly the same (unless a phase) for the forward and backward dynamics.

Figure 2 displays the LEs as functions of τ for 5CB under $\mathcal{H}_{xx}$ and $\mathcal{H}_{DQ,1}$. The decay of the LE under $\mathcal{H}_{xx}$ shows two well-defined temporal regimes, where the slope changes drastically. A short-time regime ($\tau<50$ μs) characterized by a fast decay and a long-time regime with a decay rate one order of magnitude lower than the first one. The short-time behavior can be assigned to the dipolar interactions in the molecular core, i.e., the biphenyl group including the α carbon of the aliphatic tail. There are two main observations that lead us to this assumption. First, the effective dipolar couplings in the core are much stronger than those in the aliphatic tail [32,34]. Second, we show on Sec. IV B that at times on the order of 50 μs, only half of the spins of the molecule are correlated, (see Fig. 8). We should emphasize that the motion of the nuclei in the tails is too fast ($\tau_{\text{tails}} \sim 10^{-9}$s) compared with the relevant times of this experiment (1–100 μs) and consequently the motionally averaged dipolar interactions during the forward and backward dynamics are the same. In contrast, the collective motions that produce the director fluctuations are much slower with a characteris-

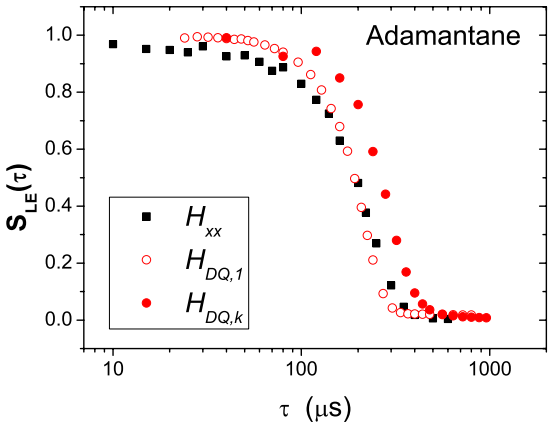

FIG. 3. (Color online) Loschmidt Echo, $S_{LE}(\tau)$, for dipolar and DQ pulse sequences in adamantane, normalized with a reference FID recorded after a $\pi/2$ pulse. Note the logarithmic time scale to emphasize the short-time behavior.

tic time τ_{OFD} that range from 1–100 μs [31,35], and they are likely to produce different average couplings during the forward and backward dynamics. This difference is apparently enhanced by the effect of the rf during the spin-lock because this liquid crystal has a large electric dipole that tends to orient with the electric field of the rf producing heat dissipation [36]. The slow decay observed for long times is associated with the finite size of the 5CB molecule that prevents the growth of high coherence orders, which are more fragile toward decoherence.

On the other hand the evolution of S_{LE} under the $\mathcal{H}_{DQ,1}$ dynamics presents a smooth sigmoidal curve. It should be emphasized that the long-time behavior of this sequence $\tau > 150$ μs is not reliable, as the long interpulse duration starts to violate the assumptions of the average Hamiltonian construction. The LE under $\mathcal{H}_{DQ,1}$ falls to 50% of its initial value for times $\tau \approx 100$ μs while the corresponding time for $\mathcal{H}_{xx}$ is $\tau \approx 50$ μs. The short-time behavior of the LE under $\mathcal{H}_{DQ,1}$ is slower than that of the LE under $\mathcal{H}_{xx}$, probably due to the effects of the spin-lock mentioned above (noninverted nonsecular terms and heating).

Figure 3 shows the LEs for adamantane in the dipolar and double-quantum cases. It can be observed that the evolutions under Hamiltonians $\mathcal{H}_{xx}$ (filled squares) and $\mathcal{H}_{DQ,1}$ (open circles) are similar. The behavior is smooth with a sigmoidal shape, falling to 50% of each initial value at $\tau \approx 200$ μs. In this compound we also measured the LE under a double-quantum Hamiltonian generated by repeating k blocks of $\tau_{DQ}^{\text{cycle}} = 60$ μs, $\mathcal{H}_{DQ,k}$. This Hamiltonian is suitable to observe the long-time behavior, while the Hamiltonian using a single block of variable interpulse times, $\mathcal{H}_{DQ,1}$, is only useful to study short times but offers the possibility to acquire intermediate points in this regime. LEs obtained from both experiments superimpose up to $\tau \approx 120$ μs, corresponding to $k=2$ blocks of $\mathcal{H}_{DQ,k}$. For longer times the LE obtained with $\mathcal{H}_{DQ,1}$ decreases more quickly than the other.

Finally, we observe that no long tail appears for any of the Hamiltonians implemented in adamantane, as occurs in 5CB for $\mathcal{H}_{xx}$. This characteristic can be probably assigned to the infinite character of the coupling network in adamantane. In this case, as we will show below, very high orders of coherences are generated.

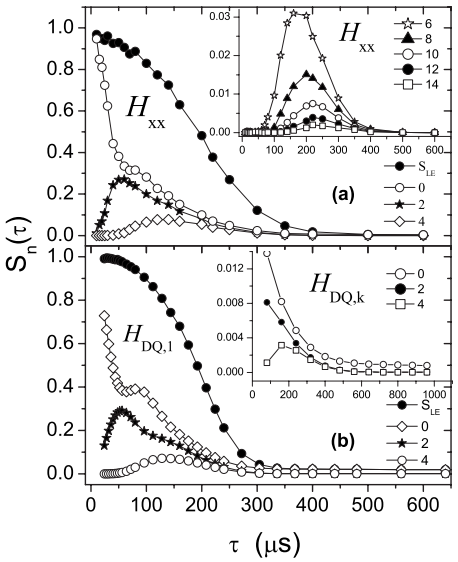

FIG. 4. Coherence order distribution $S_n(\tau)$ for $n=0,2,\ldots,14$, as a function of τ corresponding to: (a) dipolar and (b) DQ dynamics in adamantane. The inset in (b) shows coherence orders for $\mathcal{H}_{DQ,k}$ with $\tau_{DQ}^{\text{cycle}} = 120$ μs.

B. Coherence order evolution and spin counting

Figure 4 shows the evolution of the different coherence orders, $S_n(\tau)$, with dipolar and DQ Hamiltonians for adamantane. As mentioned before, normalization was performed with a reference FID recorded after a $\pi/2$ pulse. Figure 4(a) shows low coherence orders for $\mathcal{H}_{xx}$ including in the inset orders ranging from $S_6(\tau)$–$S_{14}(\tau)$. Note that as the evolution time τ increases, higher order coherences build up at the expense of the lower ones. As can be observed, the maximum intensity in the $S_n(\tau)$ curves decreases with the coherence order n. A short-time oscillation between $S_0(\tau)$ and $S_2(\tau)$ is marginally observed, corresponding to single and two spin correlations [18]. Figure 4(b) shows coherence orders from 0 to 4 for $\mathcal{H}_{DQ,1}$ while the inset shows the same coherence orders for $\mathcal{H}_{DQ,k}$ with $\tau_{DQ}^{\text{cycle}} = 120$ μs. Notice that the initial gap in the evolution under $\mathcal{H}_{DQ,1}$ [Fig. 4(b)] is due to the minimum block duration in the eight-pulse sequence, i.e., $\tau_{DQ} = 36$ μs. The usual procedure of increasing blocks instead of increasing separation between pulses, usually used for studying long-time regimes, masks the oscillating behavior observed in Fig. 4(b), as compared with its inset. Additionally, by comparing Figs. 4(a) and 4(b), it can be seen that the short-time behaviors of S_n are similar for the dipolar and DQ evolutions.

Figure 5 displays the evolutions of the coherence orders under dipolar and DQ Hamiltonians corresponding to 5CB. The short-time oscillations in $S_0(\tau)$ and $S_2(\tau)$ occurring under both dynamics are evidence of single- and two-spin correlations corresponding to strongly coupled spins in the molecule [32]. In the case of the dipolar Hamiltonian, the maximum in $S_2(\tau)$ occurs around $\tau = 40$ μs, while the local

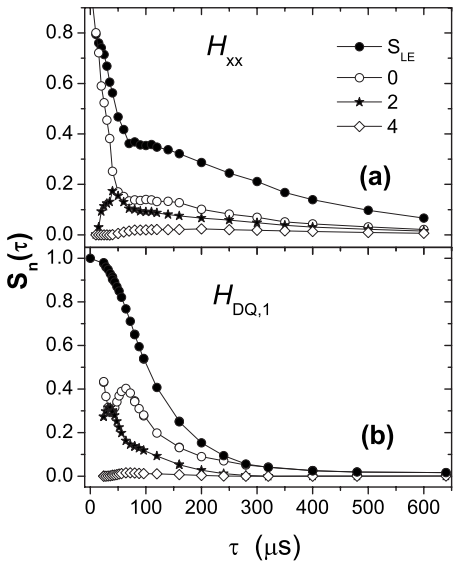

FIG. 5. Coherence order distribution $S_n(\tau)$ for $n=0$, 2, and 4, as a function of τ corresponding to (a) the dipolar and (b) DQ dynamics in 5CB.

minimum for $S_0(\tau)$ is at 70 μs [see Fig. 5(a)]. In contrast, under $\mathcal{H}_{DQ}$ evolution, S_0 and S_2 reach their local minimum and maximum at the same time [see Fig. 5(b)] leading to a smooth sigmoidal shape for the LE in this case.

One noticeable difference between the two analyzed Hamiltonians ($\mathcal{H}_{xx}$ and $\mathcal{H}_{DQ}$) is that the pathways through Liouville space are more limited for $\mathcal{H}_{DQ}$ than for $\mathcal{H}_{xx}$ [37]. This fact can be associated with the time for the development of new coherence orders that is shorter for $\mathcal{H}_{xx}$ than for $\mathcal{H}_{DQ}$. This is clearly observed in adamantane, an homogeneous and infinite system, where coherence orders 8 to 16 show a delay when evolving under $\mathcal{H}_{DQ}$ as compared with $\mathcal{H}_{xx}$ (see Fig. 6). In contrast, this is not observed in 5CB due to the small number of interacting spins.

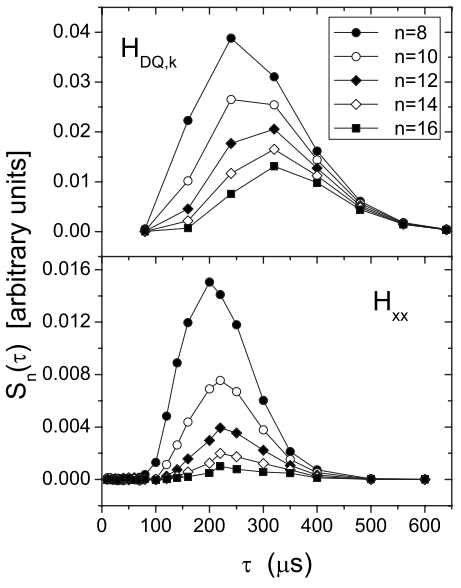

FIG. 6. Coherence orders 8 to 16 develops easily in evolution under $\mathcal{H}_{xx}$ Hamiltonian than under $\mathcal{H}_{DQ}$.

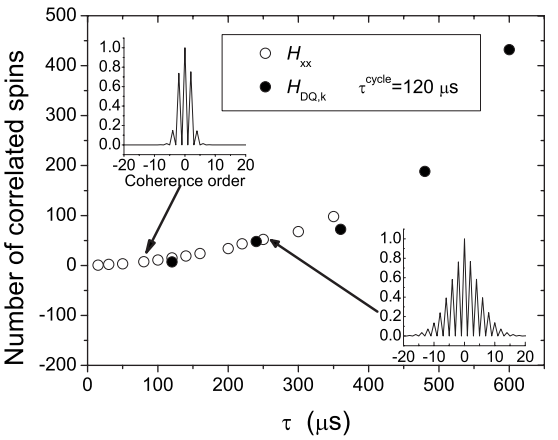

FIG. 7. Effective number of correlated spins, $N_{\text{eff}}(\tau)$ for adamantane during dipolar and DQ evolution. The insets show examples of the distribution of the signals into different coherence orders.

The number of correlated spins at a particular evolution time τ determines the shape of $S_n(\tau)$ as a function of n. In particular, the distribution becomes wider when higher coherence orders are excited. The cluster size of correlated spins can be determined from the assumption that the different coherence orders are excited with the same probability [16,17]. For a finite cluster of size N the integrated spectral intensity per order can be related to the number of multiple-quantum transitions within that order. From combinatorial arguments, the number of n quantum transitions in an N spin system is $2N!/(N-n)!(N+n)!$. For $N>6$, the distribution of coherence orders at a given time τ approaches a Gaussian $S_n(\tau)\sim\exp-n^2/N_{\text{eff}}(\tau)$. Then, the effective number of spins $N_{\text{eff}}(\tau)$ correlated during the evolution period τ can be roughly associated with the variance of the distribution.

Figures 7 and 8 display the effective number of correlated spins $N_{\text{eff}}(\tau)$ during the evolution under $\mathcal{H}_{xx}$ and $\mathcal{H}_{DQ}$ for adamantane, and under $\mathcal{H}_{xx}$ for 5CB, respectively. The insets show the distribution of the signal into different coherence orders for a couple of arbitrary times. The functional forms

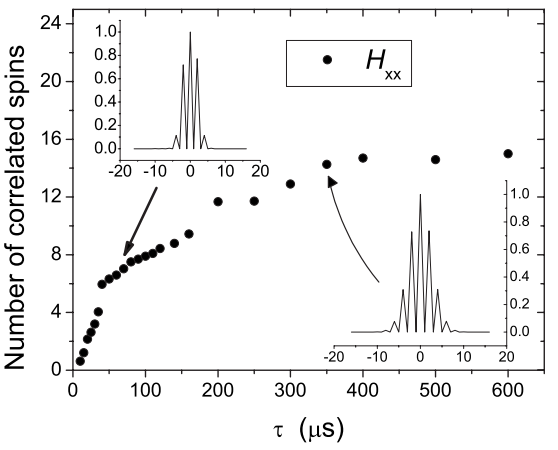

FIG. 8. Effective number of correlated spins, $N_{\text{eff}}(\tau)$ for 5CB during dipolar evolution. The insets show the distribution of the signals into different coherence orders.

of the growth of $N_{\text{eff}}(\tau)$ are clearly different among the two systems, reflecting the extent of each interaction network. The effective spin cluster size in adamantane grows uniformly under both evolutions, dipolar and DQ. On the other hand in 5CB under dipolar evolution $N_{\text{eff}}(\tau)$ grows in two steps: an initial fast increase during the first 50 μs that leads to $N_{\text{eff}} \sim 8$ spins, then a slower regime reaching a saturation value of $N_{\text{eff}} \sim 16$ after approximately 400 μs. This evidences a hierarchy in the set of dipolar couplings, i.e., the first part of the dynamics is due to the thermalization between protons in the aromatic rings and at long times the connection with all the molecule is taking place. The fact that $N_{\text{eff}}(\tau)$ stabilizes at $N_{\text{eff}} \sim 16$ instead of $N=19$ may be due to an almost self-decoupled methyl group or to an artifact in the determination of the width of the distributions. Notice that for the long times where all the spins of the molecule should appear, the signal-to-noise ratio is approximately 10 times weaker than in the short-time regime.

C. Numerical simulations for the 5CB core

In order to compare with the experiments, we performed numerical calculations of the evolutions under dipolar and double-quantum Hamiltonians for the 5CB molecule. We considered the evolution of 10 spins, eight of them belonging to the biphenyl group and the other two belonging to the first methylene group in the aliphatic chain. Motional averaged dipolar couplings for 5CB have been taken from literature [32,38]. The time dependent density matrix was calculated as $\rho(t)=\exp(-i\mathcal{H}t/\hbar)\rho(0)\exp(i\mathcal{H}t/\hbar)$, where the initial condition was $\rho(0) \propto I^z$. Then, $\rho(t)$ follows the evolution under the Hamiltonians $\mathcal{H}_{xx}$ or $\mathcal{H}_{DQ,1}$. The different coherence orders were calculated considering $S_n(t)=\Sigma_{r,s}\langle r|\rho(t)|s\rangle$ where the sum runs over the pairs r,s such that $M_z(r)-M_z(s)=n$ [15].

If decoherence is not introduced *ad hoc* in the numerical calculations, the LE at different times are built using unitary evolutions leading to conservation of the total signal, $S_{LE}(\tau)=1$. Then, in order to compare numerical and experimental results, we normalize the measured coherence orders with the global decoherence given by the LE, leading to $\bar{S}_n(\tau)=S_n(\tau)/S_{LE}(\tau)$. Figures 9 and 10 display the experimental and simulated $\bar{S}_n(\tau)$ for 5CB under dipolar and double-quantum evolutions, respectively.

In Fig. 9(a) the experimental data corresponding to dipolar evolution show that the minimum and maximum in $\bar{S}_0$ and $\bar{S}_2$, respectively, occurs at 50 μs. In quite good agreement with this result, our numerical calculations show that the first oscillation in the lowest coherence orders appears at $\tau \sim 35$ μs [see Fig. 9(b)] although none of the oscillations observed here survive the experimental decoherence. Nevertheless, there is an excellent agreement in the asymptotic behavior after $\tau \sim 300$ μs. This fact indicates that the dipolar dynamics in 5CB is dominated by the strong interactions occurring in the two biphenyl rings and the first methylene group of the aliphatic chain.

In Fig. 10, corresponding to double-quantum dynamics, it is possible to see that the experimental and numerical short-time evolutions of $\bar{S}_0$ and $\bar{S}_2$ show a coincident oscillation at approximately $\tau \sim 33$ μs. On the other hand the experimental behavior for $\bar{S}_n$ at long times can be understood considering that the effective Hamiltonian theory is not appropriate when the separation between pulses is greater than $\Delta \gtrsim 20$ μs. For $\tau > 300$ μs there is a collapse of all coherence orders into the $\bar{S}_0$. Then numerical and experimental results for DQ dynamics cannot be compared at long times by our approach.

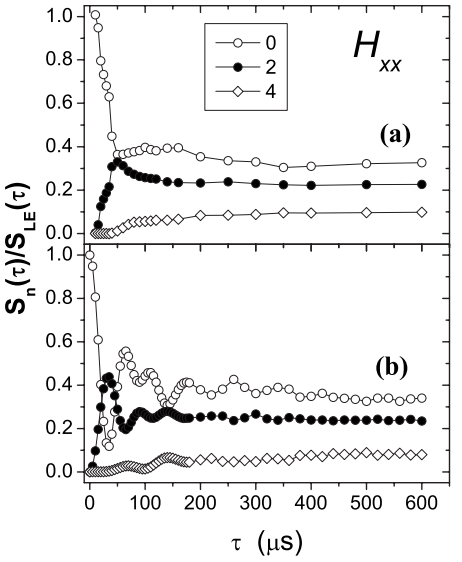

FIG. 9. Comparison between (a) experimental and (b) simulated normalized coherence orders $\bar{S}_n(\tau)$ for dipolar dynamics in 5CB.

V. CONCLUSIONS

In this work we studied the decoherence processes for nuclear-spin systems under different experimental conditions

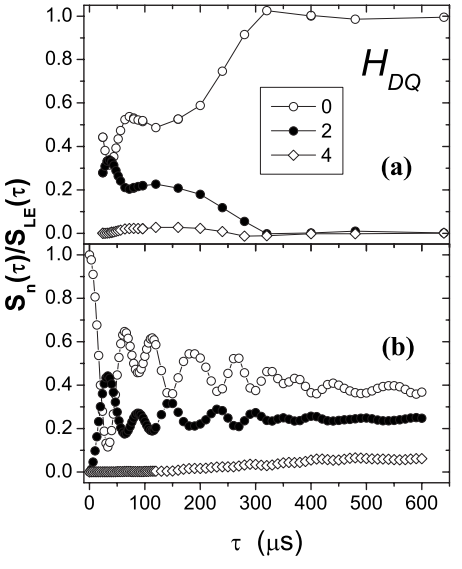

FIG. 10. Comparison between (a) experimental and (b) simulated normalized coherence orders $\bar{S}_n(\tau)$ for double-quantum dynamics in 5CB.

by inspection of the evolution of the LE. This is a simple tool that has the advantage of being acquired as a single one-dimensional experiment, in contrast with the usual two-dimensional experiment needed to obtain different coherence orders. Then, it is possible to obtain a direct idea on the pulse sequence performance and on the decoherence produced from the interaction between the quantum system and its environment. Additionally, the LE can provide an insight about the set of interactions of the studied systems.

We observed that the normalization with the LE unmasks the actual evolution of the different coherence orders, in particular for long times. Simulations in 5CB with a 10-spin system, in which the aliphatic tail has been disregarded, provide a very accurate description of the experimental results validating both, our numerical approach and the performance of the pulse sequence for dipolar evolution at long times. The agreement of the coherence order intensities between simulation and experiments for long times leads to the conclusion that the decoherence mechanism in this system affects in the same manner all the coherence orders. As a consequence, the information of the distribution of correlations of the different states is proportionally conserved even when the overall signal has decayed to 10% of its initial value. This fact is in contrast with the behavior of an infinite system, as adamantane, where the higher coherence orders are more sensitive to the decoherence effects than the lower ones.

ACKNOWLEDGMENTS

We acknowledge the financial support received from Fundación Antorchas, CONICET, FoNCyT, SeCyT-UNC, and the Partner Group for NMR Spectroscopy with High Spin Polarization with the Max Planck Institute for Polymer Research, Mainz, Germany.

[1] C. H. Bennett and D. P. DiVincenzo, Nature (London) **404**(6775), 247 (2000).
[2] J. R. Petta, A. C. Johnson, J. M. Taylor, E. A. Laird, A. Yacoby, M. D. Lukin, C. M. Marcus, M. P. Hanson, and A. C. Gossard, Science **309**, 2180 (2005).
[3] M. V. G. Dutt, L. Childress, J. Liang, E. Togan, J. Maze, F. Jelezko, A. S. Zibrov, P. R. Hemmer, and M. D. Lukin, Science **316**, 1312 (2007).
[4] D. D. Awschalom and M. E. Flatté, Nat. Phys. **3**, 153 (2007).
[5] M. Moodley and F. Petruccione, Phys. Rev. A **79**, 042103 (2009).
[6] K. C. Nowack, F. H. L. Koppens, Y. V. Nazarov, and L. M. K. Vandersypen, Science **318**, 1430 (2007).
[7] W. H. Zurek, Rev. Mod. Phys. **75**, 715 (2003).
[8] W. H. Zurek, F. M. Cuchietti, and J. P. Paz, Acta Phys. Pol. B **38**, 1685 (2007).
[9] S. Bertaina, S. Gambarelli, T. Mitra, B. Tsukerblat, A. Müller, and B. Barbara, Nature (London) **453**, 203 (2008).
[10] H. G. Krojanski and D. Suter, Phys. Rev. Lett. **93**, 090501 (2004).
[11] H. G. Krojanski and D. Suter, Phys. Rev. Lett. **97**, 150503 (2006).
[12] H. J. Cho, P. Cappellaro, D. G. Cory, and C. Ramanathan, Phys. Rev. B **74**, 224434 (2006).
[13] P. R. Levstein, G. Usaj, and H. M. Pastawski, J. Chem. Phys. **108**, 2718 (1998).
[14] G. Usaj, H. M. Pastawski, and P. R. Levstein, Mol. Phys. **95**, 1229 (1998).
[15] R. R. Ernst, G. Bodenhausen, and A. Wokaun, *Principles of Nuclear Magnetic Resonance in One and Two Dimensions* (Oxford University Press, Oxford, 1987).
[16] J. Baum, M. Munowitz, A. N. Garroway, and A. Pines, J. Chem. Phys. **83**, 2015 (1985).
[17] J. Baum and A. Pines, J. Am. Chem. Soc. **108**, 24 (1986).
[18] H. Cho, T. D. Ladd, J. Baugh, D. G. Cory, and C. Ramanathan, Phys. Rev. B **72**, 054427 (2005).
[19] P. Cappellaro, C. Ramanathan, and D. G. Cory, Phys. Rev. A **76**, 032317 (2007).
[20] C. M. Sánchez, H. M. Pastawski, and P. R. Levstein, Physica B **398**, 472 (2007).
[21] E. Rufeil-Fiori, C. M. Sánchez, F. Y. Oliva, H. M. Pastawski, and P. R. Levstein, Phys. Rev. A **79**, 032324 (2009).
[22] L. Buljubasich, G. A. Monti, R. H. Acosta, C. J. Bonin, C. E. González, and R. C. Zamar, J. Chem. Phys. **130**, 024501 (2009).
[23] O. N. Antzutkin and R. Tycko, J. Chem. Phys. **110**, 2749 (1999).
[24] K. Saalwächter, P. Ziegler, O. Spyckerelle, B. Haidar, A. Vidal, and J.-U. Sommer, J. Chem. Phys. **119**, 3468 (2003).
[25] R. A. Jalabert and H. M. Pastawski, Phys. Rev. Lett. **86**, 2490 (2001).
[26] H. Cho, D. G. Cory, and C. Ramanathan, J. Chem. Phys. **118**, 3686 (2003).
[27] C. P. Slichter, *Principles of Magnetic Resonance* (Springer, New York, 1992).
[28] K. Saalwächter, Prog. Nucl. Magn. Reson. Spectrosc. **51**, 1 (2007).
[29] M. A. Voda, D. E. Demco, J. Perlo, R. A. Orza, and B. Blümich, J. Magn. Reson. **172**, 98 (2005).
[30] I. Schnell and H. W. Spiess, J. Magn. Reson. **151**, 153 (2001).
[31] R. Y. Dong, *Nuclear Magnetic Resonance of Liquid Crystals* (Springer, New York, 1997).
[32] B. Stevensson, A. V. Komolkin, D. Sandström, and A. Maliniak, J. Chem. Phys. **114**, 2332 (2001).
[33] S. I. Doronin, I. I. Maksimov, and E. B. Fel'dman, J. Exp. Theor. Phys. **91**, 597 (2000).
[34] A. K. Chattah, G. A. Álvarez, P. R. Levstein, F. M. Cucchietti, H. M. Pastawski, J. Raya, and J. Hirschinger, J. Chem. Phys. **119**, 7943 (2003).
[35] O. Mensio, R. C. Zamar, E. Anoardo, R. H. Acosta, and R. Y. Dong, J. Chem. Phys. **123**, 204911 (2005).
[36] A. K. Chattah, F. M. Cucchietti, M. Hologne, J. Raya, and P. R. Levstein, Magn. Reson. Chem. **40**, 772 (2002).
[37] M. Munowitz, *Coherence and NMR* (Wiley, New York 1988).
[38] H. H. Segnorile, C. J. Bonin, C. E. Gonzalez, R. H. Acosta, and R. C. Zamar, Solid State Nucl. Magn. Reson. (to be published).